Easy excited state trapping and record T_{TIESST} (250 K) in a spin crossover polyanionic Fe^{II} trimer

Verónica Gómez,[†] Cristina Sáenz de Pipaón,[†] Pilar Maldonado-Illescas,[†] João Carlos Waerenborgh,[‡] Eddy Martin,[†] Jordi Benet-Buchholz,[†] and José Ramón Galán-Mascarós*[,†,¶]

Institute of Chemical Research of Catalonia (ICIQ), Av. Paisos Catalans 16, E-43007 Tarragona, Spain, Centro de Ciências e Tecnologias Nucleares, Instituto Superior Técnico, Universidade de Lisboa, 2695-066 Bobadela LRS, Portugal, and Catalan Institution for Research and Advanced Studies (ICREA), Passeig Lluis Companys, 23, E-08010, Barcelona, Spain

Received July 28, 2015; E-mail: jrgalan@iciq.es

Abstract: Reaction of the polysulfonated triazole ligand L = 4-(1,2,4-triazol-4-yl)ethanedisulfonate) with iron(II) salts in water yields the trimeric species $[Fe_3(\mu\text{-}L)_6(H_2O)_6]^{6-}$. This polyanion can be isolated from solution as the dimethylammonium salt yielding a complex hydrogen bonded network connecting anions, cations and solvent molecules in the solid state. This material shows a thermally induced spin transition for the central Fe position in the trimer above room temperature with a large hysteresis cycle (> 85 K) and remarkably slow dynamics. This allows easy quenching of the metastable high spin (HS) state via slow cooling (5 K min^{-1}). Once it is trapped, the HS state remains metastable. Thermal energy is not able to promote relaxation into the low spin (LS) ground state up to 215 K, with a characteristic T_{TIESST} = 250 K, the highest temperature ever observed for thermal trapping of an excited spin state.

Iron(II) complexes displaying spin crossover (SCO), a phenomenon in which the spin state of the metal center switches between low-spin (LS) and high-spin (HS) under external stimuli, have been the subject of many studies during the last decades. [1–5] SCO is particularly appealing in the octahedral Fe^{II} case, because the spin transition from diamagnetic $S = 0$ to paramagnetic $S = 2$ provokes a dramatic change also in color (from pink/red to white/yellow) and size (increment of 10-15% in the metal to ligand bonding distances). Besides, if this transition occurs with hysteresis a memory effect is conferred. In very recent years there is a renaissance of SCO materials in molecular magnetism [6–12] because, in contrast with other bistable species such as single molecule magnets, [13,14] SCO may occur at room temperature. Thus SCO appears specially suited for applications as stimuli-responsive molecular switches for multifunctional materials, memories, electrical circuits or display devices. [15–27]

Most reported complexes with hysteretic SCO are mononuclear or polymeric Fe^{II} compounds, typically with neutral or cationic overall charge. Our group has focused in the search for anionic SCO complexes to increase their processing capabilities when incorporated into hybrid materials. With this in mind, we have prepared sulfonated 1,2,4-triazole derivatives as building blocks. [28,29] Here, we report the SCO behavior of the polyanionic Fe^{II} SCO complex $[Fe_3(\mu\text{-}L)_6(H_2O)_6]^{6-}$ (L^{2-} = 4-(1,2,4-triazol-4-yl)ethanedisulfonate, Figure S1). As the corresponding $(Me_2NH_2)^+$ salt, this complex exhibits a spin transition above room temperature with a very large thermal hysteresis loop. Furthermore, the HS state can be easily trapped when cooling down at slow rates (> 5 K min^{-1}), remaining in its metastable state up to the highest temperatures ever observed, close to room temperature.

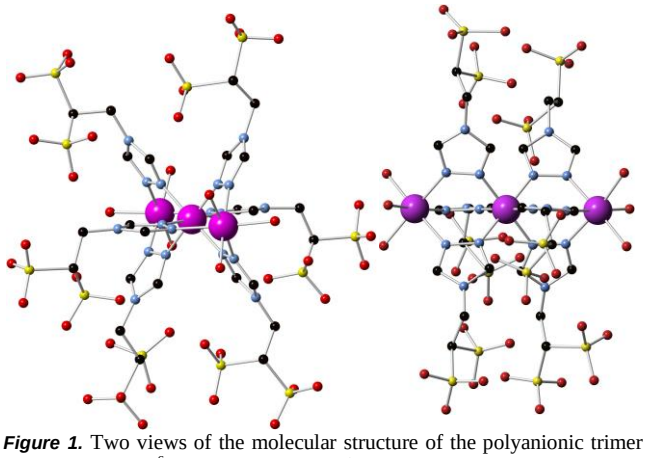

Figure 1. Two views of the molecular structure of the polyanionic trimer $[Fe_3(\mu\text{-}L)_6(H_2O)_6]^{6-}$ (H-atoms omitted for clarity). Color code: Fe = purple; S = yellow; O = red; N = blue; C = black.

Reaction of L^{2-} with Fe^{II} in a 3:1 ratio in water yielded a pale pink solution. Single crystals of $(Me_2NH_2)_6[Fe_3(\mu\text{-}L)_6(H_2O)_6]$(**1**) were isolated by layering the reaction mixture with ethanol. **1** contains the trinuclear polyanion $[Fe_3(\mu\text{-}L)_6(H_2O)_6]^{6-}$, formed by a linear array of octahedral Fe^{II} ions (Fe1-Fe2-Fe1) connected by two triple μ-triazole bridges (Figure 1 and Figure S2). The terminal Fe1 position completes its N_3O_3 hexacoordination with three H_2O molecules in *f ac* conformation. The metal to ligand distances at 100 K (Table S2) indicate HS configuration for Fe1 (average Fe1–L = 2.13 Å) and LS configuration for Fe2 (average Fe2–N = 1.99 Å). The dangling sulfonate moieties from the ethane groups adopt multiple orientations participating in a complex weakly hydrogen bonded network involving the dimethylammonium cations and water molecules, with short intermolecular O–O distances (2.6–2.9 Å, Figure S3).

Magnetic susceptibility measurements were carried out in the 2–300 K range for grained single crystals of **1** (Figure 2). At room temperature, the $\chi_M T$ product is 6.37 $cm^3mol^{-1}K$, consistent with a HS-LS-HS configuration (spin-only $\chi_M T$ = 6.00 $cm^3mol^{-1}K$). On lowering the temperature, $\chi_M T$ remains constant down to 50 K, when decreases down to 0.37 $cm^3mol^{-1}K$ at 2 K. We assign this decrease to zero-field splitting (usually very small) and antiferromagnetic interactions between paramagnetic centers.

Above room temperature (Figure 2, inset), $\chi_M T$ shows a significant increase at 360 K, suggesting a spin transition to the HS-HS-HS state, reaching 7.92 $cm^3mol^{-1}K$ at 400 K. This corresponds approximately to half of the trimers undergoing the spin transition. Upon cooling again, the sample goes slowly back to the HS-LS-

[†]ICIQ
[‡]IST
[¶]ICREA

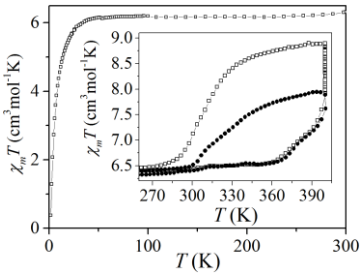

Figure 2. $\chi_m T$ vs T plots for **1** in the 2-300 K range and in the 270-400 K range (inset). Empty squares show the magnetic behavior when the sample is maintained at 400 K until saturation. These measurements were performed stabilizing the temperature for each data point (scan rate ≈ 0.1 K min^{-1}).

HS state, with a hysteresis loop of over 65 K, reaching the initial $\chi_m T$ values below 300 K. When the sample is maintained at 400 K, $\chi_m T$ keeps increasing until it saturates at 8.89 cm^{3}mol^{-1}K (Figure S4), corresponding to ≈ 84% completeness. The cooling behavior from magnetic saturation at 400 K (Figure 2inset), exhibits a hysteresis loop of 90 K ($T_{1/2}(\uparrow)$ = 400 K and $T_{1/2}(\downarrow)$ = 310 K) with a quasi-static scan rate. This is among the widest robust thermal hysteresis found for SCO materials. [30–34] This thermal hysteresis is reproducible as confirmed by the consistency of successive cycles at 1 K min^{-1} (Figure S5). The possibility of a hydration/dehydration process affecting the hysteretic behavior can be ruled out given that all measurements were done in pinched capsules to allow proper purging. In addition, analogous behavior was observed for samples previously dehydrated in an oven for 12 hours at 135°C (Figure S5) and thermal gravimetry analysis under humid air (Figure S6) confirms that **1** barely rehydrates during the cooling branch, and that water content is identical during successive cycles in the cooling or heating bench, depending only on temperature. This confirms that hydration/dehydration cannot promote appearance of a memory effect.

Since SCO can be very sensitive to scan rate, [35] we studied its effect in the hysteresis cycle (Figure 3, top). The heating branch does not change significantly with scan rate. The cooling branch deviates from "settle mode" at rates above 2 K min^{-1}. Remarkably, the spin transition becomes significantly quenched at scan rates as slow as 5 K min^{-1}. This phenomenon, the temperature-induced excited spin-state trapping (TIESST), typically requires very fast cooling (liquid nitrogen immersion). [36–40] At a 10 K min^{-1} cooling rate, 57% of the complexes are trapped as HS-HS-HS. We extracted a characteristic T_{TIESST} = 250 K (Figure 3, bottom) following the method defined by Letard *et al.* through a heating run at 0.3 K min^{-1}. [37] This is the highest T_{TIESST} reported, the previous record being 156 K. [41] At faster heating rates the HS-HS-HS state is not completely depopulated until reaching room temperature. For example, 285 K are needed at 1 K min^{-1} (Figure S7). It is important to note that the X-ray diffraction pattern does not change after multiple thermal cycles, confirming the stability of the material and also the absence of additional crystallographic phases (Figure S8).

We measured isothermal relaxation curves after keeping **1** at 400 K for 6.5 hours, and then cooling at 10 K min^{-1} down to the desired temperature (Figure 4). Relaxation exhibits sigmoidal character below 245 K, but it deviates from this behavior at higher temperatures suggesting a decrease in cooperativity. However, the plots cannot be satisfactorily modeled with a unique relaxation process (sigmoidal or stretch exponential), which suggests participation of multiple microscopic contributions. From the relaxation rate at very long times, as extracted from the linear decay of the plot tails (Figure S9), we can estimate relaxation times as long as over 8 hours at 265 K, and over 3 days at 235 K, for example. This showcases the remarkable slow dynamics characteristic of this SCO material.

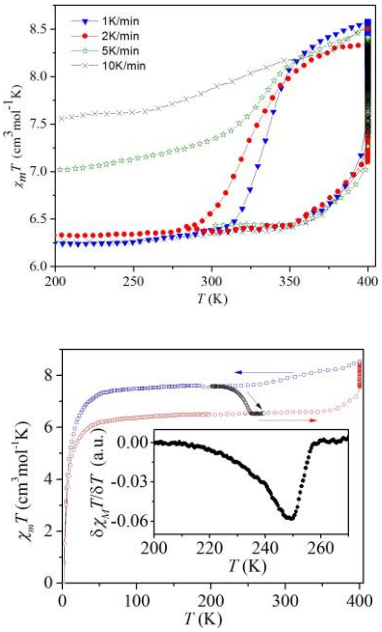

Figure 3. $\chi_m T$ vs T plots for **1** at: (top) different heating/cooling rates, allowing for saturation at 400 K; (bottom) heating up to 400 K until saturation (red circles), cooling down from saturation at 10 K min^{-1} rate (blue circles), and warming up again at 0.3 K min^{-1} (black circles). (inset) $\delta\chi_m T/\delta T$ vs T curve for the latter heating branch, whose minimum defines T_{TIESST}.

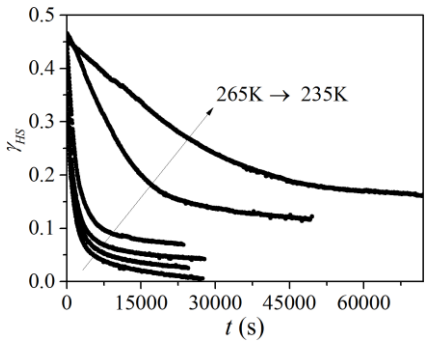

Figure 4. Isothermal relaxation curves for the HS fraction (γ_{HS}) for **1** at 265, 260, 255, 250, 240 and 235 K.

The ^{57}Fe Mössbauer data are in good agreement with the magnetic measurements. Both spectra at 295 and 4 K (Figure 5a,b) show two quadrupole doublets: one with higher quadrupole splitting (*QS*) due to HS Fe^{II} (Table 1) and the other with lower *QS* typical of LS Fe^{II}. [1] At 4 K the recoil-free fractions of LS and HS Fe^{II} are usually similar and their relative areas may be considered a good approximation of the LS and HS Fe^{II} fractions. The LS Fe^{II} relative area is slightly higher at 295 K which may be attributed to its higher recoil-free fraction when compared to HS Fe^{II} at 295 K. The ratio of the relative areas at 4 K, 2:1 within experimental accuracy, is consistent with the HS-LS-HS ground state in the 295 - 4 K temperature range. In order to study the thermally trapped metastable HS-HS-HS state, we heated a sample at 403 K during five hours, dropped it quickly into liquid nitrogen, and brought it to the cryostat. The spectrum obtained at 4 K (Figure 5c) showed that the relative area of the LS Fe^{II} doublet was reduced approximately 10% relative to the sample before heat treatment (Table 1). In addi-

Table 1. Parameters estimated from the Mössbauer spectra of the pristine and the heat treated samples of compound **1** taken at 295 and 4 K.

sample	$T(K)$	IS(mm s^{-1})[a]	QS(mm s^{-1})[b]	Γ(mm s^{-1})[c]	I(%)[d]	assignment
pristine **1**	295	0.45	0.14	0.27	39	LS
		1.14	1.98	0.41	61	HS (d1)
	4	0.52	0.19	0.28	35	LS
		1.27	2.91	0.42	65	HS(d1)
1 heated at 403 K and quenched in liquid N_2	4	0.52	0.24	0.33	25	LS
		1.29	2.91	0.43	42	HS (d1)
		1.30	2.30	0.37	11	HS (d2)
		1.25	3.38	0.35	22	HS (d3)
1 heated at 403 K, quenched in liquid N_2 and warmed up to 295 K	295	0.45	0.12	0.28	38	LS
		1.15	1.97	0.40	62	HS (d1)
	4	0.52	0.20	0.30	37	LS
		1.28	2.88	0.43	63	HS (d1)

[a]Isomer shift relative to metallic α-Fe at 295 K; [b]Quadrupole splitting; [c]Full width at half height; [d]Relative areas. d1: terminal HS Fe^{II} in HS-LS-HS configuration; d2: central HS Fe^{II} in HS-HS-HS configuration; d3: terminal HS Fe^{II} in HS-HS-HS configuration (see text). Estimated errors are $\leq$ 0.02 mm s^{-1} for *IS* and *QS* and $\leq$ 2% for *I*. The areas and widths of both peaks in a quadrupole doublet were constrained to remain equal during the refinement procedure.

tion, the HS Fe^{II} contribution could only be fitted if three doublets were considered: a first doublet (d1) with parameters similar to those of terminal HS Fe^{II} in the untreated sample; a second doublet (d2) with a relative area of$\approx$11% that could be assigned to central HS Fe^{II} (notice that 11% is within experimental accuracy equal to the relative area reduction of the central LS Fe^{II}); and a third doublet (d3), with the highest QS, which may be attributed to terminal HS Fe^{II} with a modified environment. These terminal HS Fe^{II} with the highest QS are most likely the nearest Fe neighbours of the central HS Fe^{II} in agreement with the fact that the relative area of d3 is approximately twice that of d2 and the sum of d1 and d3 relative areas is equal to the area of the HS doublet in the untreated sample. Thus, the three HS contributions to the spectra arise from the configurations HS(d1)-LS-HS(d1) and HS(d3)-HS(d2)-HS(d3). Considering that the central Fe^{II} cations are 33% of the total number of Fe cations in the compound, these results indicate quenching of one third of the molecules in this experiment. The spectrum taken after warming the quenched sample to room temperature is identical, within experimental error, to the spectrum of the untreated sample (Figure 5, Table 1), showing that the thermally quenched state decays at room temperature towards the as-prepared state. This means that all molecules are back to the HS-LS-HS ground state. The presence of two different environments for the terminal Fe^{II} positions is only observed when HS-HS-HS species are present. The spectrum taken at 4 K of the treated sample after warming to room temperature for 48 hours is indistinguishable from the 4 K spectrum of the untreated sample confirming the conclusions deduced from the 295 K spectrum, and the perfect stability (and bistability) of the sample through multiple temperature cycles.

In summary, we have isolated a novel polyanionic Fe^{II} trimer as its dimethylamonnium salt, which exhibits spin crossover behavior for its central Fe^{II} position above room temperature with a large thermal hysteresis. The spin transition dynamics are remarkably slow, allowing for an easy trapping of the excited spin state when the material is cooled down at reasonably slow rates ($>$ 5 K min^{-1}). Remarkably, this material exhibits bistability in the high temperature range (280–400 K), but also in the low temperature range (2–250 K), since the metastable HS state cannot relax back to the ground state up to very high temperatures (T_{TIESST} = 250 K). This is the highest temperature at which memory effect remains in a thermally quenched SCO system, 100 K higher than that of the previous record. It is even higher than the values displayed by Prussian blue analogues, where electron transfer kinetics play a role in the stabilization of the metastable state. [42] The extremely slow relaxation exhibited at such high temperatures opens unique possibilities for room temperature applications.

We assign the origin of such striking features to the presence of multiple sulfate groups in the ligands backbone. This is unique, since in all previous SCO materials (mostly neutral or cationic) the ligands are either neutral, or mono anionic with the charged groups directly bound to the Fe centers. In $[Fe_3(\mu\text{-}L)_6(H_2O)_6]^{6-}$, the charged peripheral groups may have an important role during the spin transition. During the HS→LS process, the shrinking to the ground state will force a direct approach between multiple sulfate groups on adjacent triazoles bridges in the complex. Thus, an activation energy arising from the electrostatic repulsion needs to be overcome. This activation energy slows the process, making it scan rate dependent, and resulting in easy quenching of the metastable state. It is worth to note that such scan rate dependence does not appear during the opposite LS→HS transition. During the latter, the distances between sulfate groups increase and a much lower activation energy is expected, taking into account only electrostatic considerations. We would also like to highlight that this molecular material is soluble and stable in water allowing for easy and convenient processing techniques to develop bistable hybrid materials at the nanoscale.

ASSOCIATED CONTENT

Supporting Information. Synthesis details, additional characterization data, including powder X-ray diffraction and additional magnetic data. This material is available free of charge via the Internet at http://pubs.acs.org.

AUTHOR INFORMATION

Corresponding Author

*jrgalan@iciq.es

Present Address

VG present address: Institute of Nanotechnology, Karlsruhe Institute of Technology (KIT), Hermann-von-Helmholtz-Platz 1, 76344 Eggenstein-Leopoldshafen, Germany.

Author Contributions

VG and CSdP both authors contributed equally to this work.

Notes

The authors declare no competing financial interest.

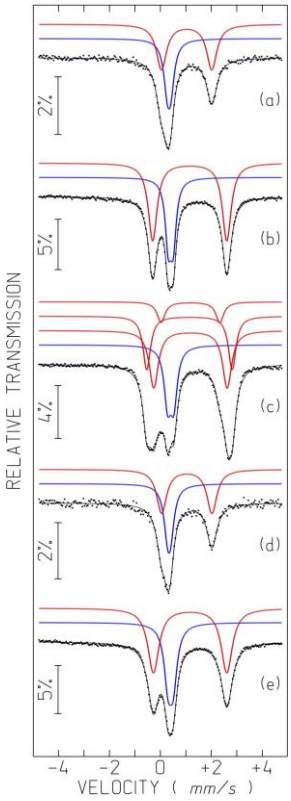

Figure 5. ^{57}Fe Mössbauer spectra of compound **1**. Spectra of pristine sample taken at (a) 295 and (b) 4 K. Spectra of sample heated at 403 K and quenched in liquid N_2, taken at (c) 4 K, (d) 295 K after warming up for 24 hours and (e) at 4 K after cooling down from 295 K. The blue and red lines refer to the LS and HS Fe^{II}, respectively.

Acknowledgement

We thank the financial support of the EU (ERC Stg grant 279313, CHEMCOMP), the Spanish Ministerio de Economía y Competitividad (MINECO) through Severo Ochoa Excellence Accreditation 2014-2018 (SEV-2013-0319) and the ICIQ Foundation.

References

(1) Gütlich, P.; Garcia, Y.; Goodwin, H. A. *Chem. Soc. Rev.* **2000**, *29*, 419–427.
(2) Bousseksou, A.; Molnar, G.; Salmon, L.; Nicolazzi, W. *Chem. Soc. Rev.* **2011**, *40*, 3313–3335.
(3) Carmen Munoz, M.; Real, J. A. *Coord. Chem. Rev.* **2011**, *255*, 2068–2093.
(4) Aromí, G.; Barriosa, L. A.; Roubeau, O.; Gamez, P. *Coord. Chem. Rev.* **2010**, *255*, 485–546.
(5) Halcrow, M. A. *Chem. Soc. Rev.* **2011**, *40*, 4119–4142.
(6) Gütlich, P. *Eur. J. Inorg. Chem.* **2013**, 581–591.
(7) Quintero, C. M.; Félix, G.; Suleimanov, I.; Sánchez Costa, J.; Molnar, G.; Salmon, L.; Nicolazzi, W.; Bousseksou, A. *Beilstein J. Nanotechnol.* **2014**, *5*, 2230–2239.
(8) Costa, J. S.; Rodríguez-Jiménez, S.; Craig, G. A.; Barth, B.; Beavers, C. M.; Teat, S. J.; Aromí, G. *J. Am. Chem. Soc.* **2014**, *136*, 3869–3874.
(9) Prins, F.; Monrabal-Capilla, M.; Osorio, E. A.; Coronado, E.; van der Zant, H. S. J. *Adv. Mater.* **2011**, *23*, 1545–1549.
(10) Miyamachi, T.; Gruber, M.; Davesne, V.; Bowen, M.; Boukari, S.; Joly, L.; Scheurer, F.; Rogez, G.; Yamada, T. K.; Ohresser, P.; Beaurepaire, E.; Wulfhekel, W. *Nat Commun* **2012**, *3*, 938.
(11) Ohkoshi, S.; Imoto, K.; Tsunobuchi, Y.; Takano, S.; Tokoro, H. *Nat. Chem.* **2011**, *3*, 564–569.
(12) Samanta, S.; Demesko, S.; Dechert, S.; Meyer, F. *Angew. Chem. Int. Ed.* **2015**, *54*, 583–587.
(13) Sessoli, R.; Powell, A. *Coord. Chem. Rev.* **2009**, *253*, 2328–2341.
(14) Bogani, L.; Wernsdorfer, W. *Nat. Mater.* **2008**, *7*, 179–186.
(15) Matsumoto, T.; Newton, G. N.; Shiga, T.; Hayami, S.; Matsui, Y.; Okamoto, H.; Kumai, R.; Murakami, Y.; Oshio, H. *Nat. Commun.* **2014**, *5*, 3865.
(16) Aravena, D.; Ruiz, E. *J. Am. Chem. Soc.* **2012**, *134*, 777–779.
(17) Craig, G. A.; Roubeau, O.; Aromí, G. *Coord. Chem. Rev.* **2015**, *269*, 13–31.
(18) Warner, B.; Oberg, J. C.; Gill, T. G.; El Hallak, F.; Hirjibehedin, C. F.; Serri, M.; Heutz, S.; Arrio, M.-A.; Sainctavit, P.; Mannini, M.; Poneti, G.; Sessoli, R.; Rosa, P. *J. Phys. Chem. Lett.* **2013**, *4*, 1546–1552.
(19) Larionova, J.; Salmon, L.; Guari, Y.; Tokarev, A.; Molvinger, K.; Molnar, G.; Bousseksou, A. *Angew. Chem. Int. Ed.* **2008**, *47*, 8236–8240.
(20) Wang, C.-F.; Li, R.-F.; Chen, X.-Y.; Wei, R.-J.; Zheng, L.-S.; Tao, J. *Angew. Chem. Int. Ed.* **2015**, *54*, 1574–1577.
(21) Koo, Y.-S.; Galan-Mascaros, J. R. *Adv. Mater.* **2014**, *26*, 6785–6789.
(22) Duriska, M. B.; Neville, S. M.; Moubaraki, B.; Cashion, J. A.; Halder, G. J.; Chapman, K. W.; Balde, C.; Letard, J. F.; Murray, K. S.; Kepert, C. J.; Batten, S. R. *Angew. Chem. Int. Ed.* **2009**, *48*, 2549–2552.
(23) Hernández, E. M.; Quintero, C. M.; Kraieva, O.; Thibault, C.; Bergaud, C.; Salmon, L.; Molnar, G.; Bousseksou, A. *Adv. Mater.* **2014**, *26*, 2889–2893.
(24) Phan, H.; Benjamin, S. M.; Steven, E.; Brooks, J. S.; Shatruk, M. *Angew. Chem. Int. Ed.* **2015**, *54*, 823–827.
(25) Ludwig, E.; Naggert, H.; Kalläne, M.; Rohlf, S.; Kröger, E.; Bannwarth, A.; Quer, A.; Rossnagel, K.; Kipp, L.; Tuczek, F. *Angew. Chem. Int. Ed.* **2014**, *53*, 3019–3023.
(26) Seredyuk, M.; Muñoz, M. C.; Castro, M.; Romero-Morcillo, T.; Gaspar, A. B.; Real, J. A. *Chem. Eur. J.* **2013**, *19*, 6591–6596.
(27) Money, V. A.; Carbonera, C.; Elhaïk, J.; Halcrow, M. A.; Howard, J. A. K.; Letard, J.-F. *Chem. Eur. J.* **2007**, *13*, 5503–5514.
(28) Gomez, V.; Benet-Buchholz, J.; Martin, E.; Galan-Mascaros, J. R. *Chem. Eur. J.* **2014**, *20*, 5369–5379.
(29) Gomez, V.; Lillo, V.; Escudero-Adan, E. C.; Martin, E.; Galan-Mascaros, J. R. *Dalton Trans.* **2013**, *42*, 6374–6380.
(30) Halcrow, M. A. *Chem. Lett.* **2014**, *43*, 1178–1188.
(31) Lochenie, C.; Bauer, W.; Railliet, A. P.; Schlamp, S.; Garcia, Y.; Weber, B. *Inorg. Chem.* **2014**, 11563–11572.
(32) Weber, B.; Bauer, W.; Pfaffeneder, T.; Dirtu, M. M.; Naik, A. D.; Rotaru, A.; Garcia, Y. *Eur. J. Inorg. Chem.* **2011**, 3193–3206.
(33) Weber, B.; Bauer, W.; Obel, J. *Angew. Chem. Int. Ed.* **2008**, *47*, 10098–10101.
(34) Bushuev, M. B.; Daletsky, V. A.; Pishchur, D. P.; Gatilov, Y. V.; Korolkov, I. V.; Nikolaenkova, E. B.; Krivopalov, V. P. *Dalton Trans.* **2014**, *43*, 3906–3910.
(35) Kulmaczewski, R.; Olguín, J.; Kitchen, J. A.; Feltham, H. L. C.; Jameson, G. N. L.; Tallon, J. L.; Brooker, S. *J. Am. Chem. Soc.* **2014**, *136*, 878–881.
(36) Murnaghan, K. D.; Carbonera, C.; Toupet, L.; Griffin, M.; Dirtu, M. M.; Desplanches, C.; Garcia, Y.; Collet, E.; Letard, J.-F.; Morgan, G. G. *Chem. Eur. J.* **2014**, *20*, 5613–5618.
(37) Paradis, N.; Chastanet, G.; Letard, J.-F. *Eur. J. Inorg. Chem.* **2012**, *2012*, 3618–3624.
(38) Garcia, Y.; Ksenofontov, V.; Mentior, S.; Dirtu, M.; Gieck, C.; Bhatthacharjee, A.; Gütlich, P. *Chem. Eur. J.* **2008**, *14*, 3745–3758.
(39) Craig, G. A.; Sánchez Costa, J.; Roubeau, O.; Teat, S. J.; Aromí, G. *Chem. Eur. J.* **2011**, *17*, 3120–3127.
(40) Craig, G. A.; Costa, J. S.; Roubeau, O.; Teat, S. J.; Shepherd, H. J.; Lopes, M.; Molnar, G.; Bousseksou, A.; Aromí, G. *Dalton Trans.* **2013**, *43*, 729–737.
(41) Wang, H.; Sinito, C.; Kaiba, A.; Costa, J. S.; Desplanches, C.; Dagault, P.; Guionneau, P.; Letard, J.-F.; Négrier, P.; Mondieig, D. *Eur. J. Inorg. Chem.* **2014**, *2014*, 4927–4933.
(42) Li, D.; Clerac, R.; Roubeau, O.; Harté, E.; Mathoniere, C.; Le Bris, R.; Holmes, S. M. *J. Am. Chem. Soc.* **2008**, *130*, 252–258.